10.1515/astro-2017-0150

Baltic Astronomy, vol. 22, 101–110, 2013

ON THE SPECTRUM OF EXTREMELY METAL-POOR STAR HD 52961

Tõnu Kipper
Tartu Observatory, Tõravere, 61602, Estonia; tk@aai.ee

Received: 2013 April 19; accepted: 2013 May 21

Abstract. High resolution spectra of the extremely metal-poor star HD 52961 are investigated. The atmospheric parameters found are: $T_{\rm eff} = 6000 \pm 100$ K, $\log g = 0.5 \pm 0.5$, $\xi_{\rm t} = 6.8$ km s^{-1}, [Fe/H] = –4.50± 0.20. The carbon abundance is close to the solar one, [C/H] = -0.17 ± 0.12. At the same time abundances of heavy refractory elements are very low. The chemical composition and atmospheric parameters have not changed compared to the first observations of the star about 20 years ago, contrary to expectation of dissolving the peculiarities by mass-loss during a relatively short time. We also find evidence of ongoing mass-loss in this post-AGB star with a rate of $\dot{M} \approx 5 \cdot 10^{-6}\, M_{\odot}\, {\rm yr}^{-1}$.

Key words: stars: atmospheres – stars: individual: HD 52961

1. INTRODUCTION

HD 52961 (= PS Gem) is a post-AGB star with very low metallicity discovered by Waelkens et al. (1990). HD 52961 is a RV Tauri like star, similar to RV_b objects. Its metallicity estimated by Waelkens et al. (1991) is [Fe/H] = –4.8.

Table 1. Basic parameters of PS Gem = HD 52961 (SIMBAD database).

Coordinates	$\alpha_{\rm J2000}$	07 03 39.63
	$\delta_{\rm J2000}$	10 46 13.06
Galactic coordinates	l	204.6705°
	b	7.5746°
Mean magnitude	B	7.76
	V	7.37
IRAS fluxes (Jy)		
	12 μm	4.53
	25 μm	2.22
	60 μm	0.95
	100 μm	0.87
Spectral type		A0
Parallax π (mas)		0.02 ± 0.56
Distance d (kpc)		2.1 ± 0.4

They also performed *JHKLM* photometry of HD 52961. The post-AGB nature of HD 52961 was revealed by its excess in the near-IR and at the IRAS wavelengths. Using these data Waelkens et al. (1991) modeled the circumstellar dust envelope and estimated the basic parameters of the HD 52961 atmosphere: $T_{\rm eff} = 6000$ K and $\log g = 0.5$. The basic parameters of HD 52961, as listed in the SIMBAD database, are presented in Table 1. The spectral class presented here was revised by Waelkens et al. (1991) to early F. The parallax indicated in Table 1 is that obtained by Hipparcos (Van Leeuwen 2007).

It is widely accepted that very low metallicity of HD 52961 is not primordial but is acquired by a depletion mechanism in the dusty envelope (Baker et al. 1996). The same authors also claim that the low metallicity photosphere formed by the

selective accretion of metal-poor gas can only be sustained if there is no convection or strong stellar wind. They estimate that with typical post-AGB mass-loss rate of $\dot{M} \approx 10^{-7}$ to 10^{-8} $M_{\odot}\,\mathrm{yr}^{-1}$ such photosphere would disperse in about 100 years. Therefore it would be interesting to look if during the 20 years which have passed from the first studies of HD 52961 any observable changes took place. In this note we describe the spectrum of HD 52961 using 7 ESPaDOnS spectrograms from the CFHT archive. These spectra were observed by Dinh Van Trung on 2006 February 8. The used spectral region covers the wavelength range 390–940 nm with a resolution of $R \approx 65000$. The signal-to-noise ratio of individual spectra is close to 250, it is somewhat lower at $\lambda < 500$ nm.

2. ANALYSIS

2.1. Atmospheric parameters and the used model atmospheres

Abundances of elements were derived with the help of the Kurucz program WIDTH5. As the starting basic atmospheric parameters we used those found by Waelkens et al. (1991) from their SED modeling of HD 52961: $T_{\mathrm{eff}} = 6000$ K and $\log g = 0.5$. Model atmospheres from the Kurucz grids[1] were used. From the plot of the observed Hβ line together with Kurucz's model profiles we concluded that the effective temperature and the surface gravity could be a little higher up to $T_{\mathrm{eff}} = 6250$ K and $\log g = 0.5 \div 1.0$ (Figure 1). There is no difference in the resulting profiles when using metallicities –4.5 or –5.0.

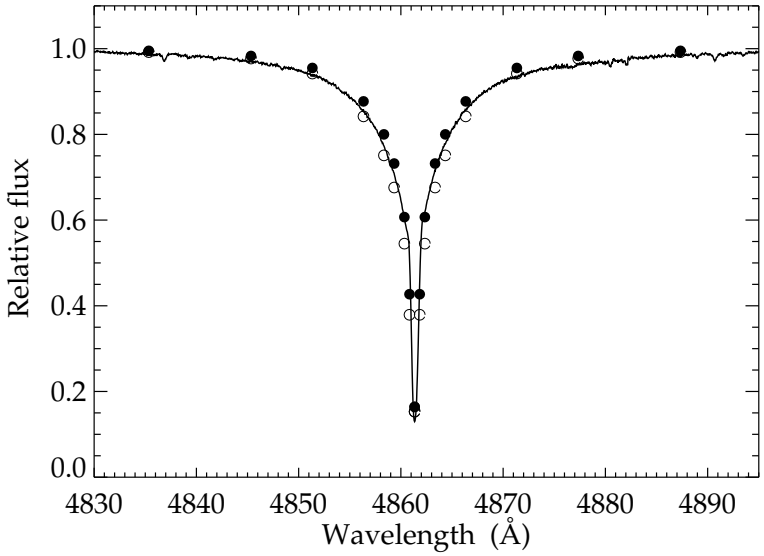

Fig. 1. The observed and calculated profiles of the Hβ line of HD 52961. The filled circles correspond to the model (6000/0.5), the open circles to the model (6250/1.0).

In the spectrum of HD 52961, we were able to identify 82 C I lines. Using this most numerous line set, by forcing the excitation equilibrium, we found the

[1] http://kurucz.harvard.edu/grids/gridm45 and /gridm50

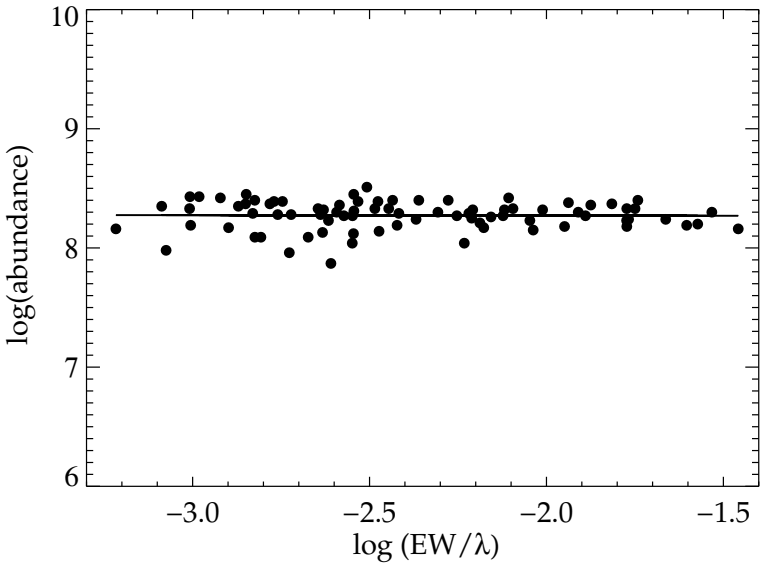

Fig. 2. The dependence of the carbon abundance on the C I line strengths. The plot is made for a microturbulent velocity of 6.8 km s^{-1}.

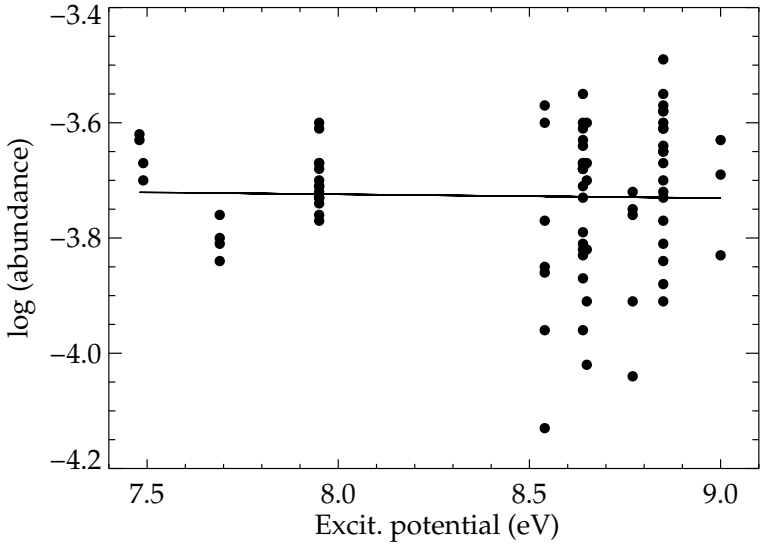

Fig. 3. The dependence of the carbon abundance on the C I line lower excitation potential. The plot is made for a microturbulent velocity of 6.8 km s^{-1} and $T_{\rm eff}$ = 6000 K.

effective temperature $T_{\rm eff} = 6000 \pm 100$ K and the microturbulent velocity $\xi_{\rm t} = 6.8$ km s^{-1} (Figures 2 and 3). With these parameters the carbon abundance is $\log \varepsilon({\rm C}) = 8.26 \pm 0.12$.

We also found a few lines of Fe I and Fe II. The iron abundances from 7 Fe I

lines is $\log\varepsilon(\mathrm{Fe}) = 2.93 \pm 0.13$ and from 3 lines of Fe II it is $\log\varepsilon(\mathrm{Fe}) = 3.10 \pm 0.05$. These abundances were found using the same $\xi_\mathrm{t} = 6.8$ km s^{-1} and $\log g = 0.5$. We consider that these abundances within the errors coincide. This supports the choice of the value of the surface gravity.

Table 2. Chemical composition of HD 52961. In Remarks the number of the used lines and the sources of oscillator strengths are indicated.

El.	Sun[1]	HD 52961		Remarks
	$\log\varepsilon$	$\log\varepsilon$	[El/H]	
H	12.00			
C	8.43	8.26 ± 0.12	–0.17	82 C I, NIST[2]
N	7.83	7.91 ± 0.04	0.08	11 N I, NIST
O	8.69	8.62 ± 0.14	–0.07	10 O I, NIST
Na	6.24	5.04 ± 0.03	–1.20	6 Na I, NIST
Mg	7.60	3.60 ± 0.08	–4.00	3 Mg I, NIST
Si	7.51	3.51	–4.00	1 Si I, NIST
S	7.12	6.62 ± 0.16	–0.45	20 S I, NIST
Ca	6.34	2.23 ± 0.41	–4.11	5 Ca II, NIST
Sc	3.15	-1.76	–4.91	1 Sc II, NIST
Ti	4.95	0.83 ± 0.87	–4.12	6 Ti II, NIST
Cr	5.64	1.85 ± 0.01	–3.72	2 Cr II, Sp.Web[3]
Mn	5.43	2.36 ± 0.14	–3.07	2 Mn I, Th.[4]
Fe	7.50	3.00 ± 0.15	–4.50	7 Fe I,3 Fe II, NIST
Ni	6.22	4.08 ± 0.11	–2.14	2 Ni I, Sp.Web, Th.
Zn	4.56	3.14 ± 0.03	–1.42	2 Zn I, Sp.Web
Sr	2.87	-1.57 ± 0.05	–4.44	2 Sr II, NIST
Ba	2.18	-2.13 ± 0.06	–4.31	2 Ba II, NIST

[1] Asplund et al. (2009), relative to $\log\varepsilon(\mathrm{H})$.
[2] NIST Atomic Spectra Database, Ralchenko et al. (2011).
[3] SpectroWeb database, Lobel (2010).
[4] Thévenin (1989) & Thévenin (1990).

2.2. Abundances

The effective temperature $T_\mathrm{eff} = 6000$ K, surface gravity $\log g = 0.5$ and microturbulent velocity $\xi_\mathrm{t} = 6.8$ km s^{-1}, found from the analysis of C I lines, were used for other elements too. The sources of oscillator strengths are indicated in Table 2, where the resulting abundances are listed. The measured equivalent widths of lines, the used oscillator strength values and the derived abundances are listed in Table 4. Most of the used oscillator strengths were taken from the NIST Atomic Spectra Database (Ralchenko et al. 2011) and from the SpectroWeb database (Lobel 2010).

We confirm the Waelkens et al. (1991) result concerning a very low iron abundance, [Fe/H] = –4.50, together with almost normal C, N, O abundances and a relatively high sulfur abundance. Here is important to note that most of the listed abundances rely only on very small number of lines, even on a single line.

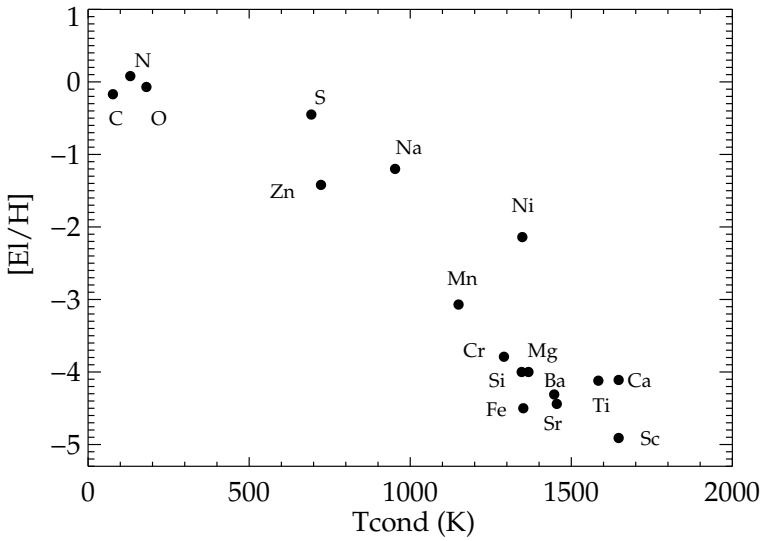

Fig. 4. Dependence of element abundances in HD 52961 on the element condensation temperature $T_{\rm cond}$ (Lodders 2003).

Table 3. Equivalent widths [pm] and heliocentric velocities [km s^{-1}] of the split line components in the spectrum of HD 52961.

Line	$W_{\rm blue}$	$V_{\rm blue}$	$W_{\rm red}$	$V_{\rm red}$
Na I 5889.97	22.8	2.0	42.4	17.7
Na I 5895.94	25.7	8.4	23.0	22.4
Ca I 4226.74	2.0	6.0	1.2	17.3
Ca II 3933.68	8.6	6.7	36.9	22.0
Ca II 3968.49	12.2	7.4	35.8	15.7
Ca II 8498.06	2.1	5.9	21.7	18.3
Ca II 8542.14	6.4	4.8	48.8	17.8
Ca II 8662.17	10.5	4.9	41.0	19.4
Sr II 4077.72	1.6	7.1	9.1	18.8
Sr II 4215.54	1.7	7.1	5.9	19.9
Ba II 4554.04	0.3	7.5	1.2	21.3
Ba II 4934.10	0.2	7.0	0.8	22.8

Therefore the errors are large. The indicated errors show only the scatter due to estimates from different lines. Taking into account these large errors, the differences in individual abundances do not differ from the Waelkens et al. (1991) results, except of the abundances of N and S, which we found to be larger by 0.4 and 0.6 dex respectively. For the blue lines of S I this change could be fully explained by differences in the used oscillator strengths, but not for the near-IR lines. On the other hand, these S I lines are quite heavily blended. Nevertheless, the severe underabundance of metals is preserved and seems to be related to the depletion via dust formation and subsequent accretion of the remaining gas to the photosphere. Such a depletion is illustrated by Figure 4 where we plot element abundances in HD 52961 versus the condensation temperature of elements (Lodders 2003).

2.3. Line splitting and radial velocities

Metallic lines originating from low excitation levels ($\chi_{\rm lower} < 1.7$ eV have absorption profiles with double dips (Figure 5).

In Table 3 all such lines are listed with the parameters of components found by the Gaussian decomposition. The rest wavelengths were taken from Roland's table (Moore et al. 1966). Excluding the very strong lines of Na I D, the mean velocity

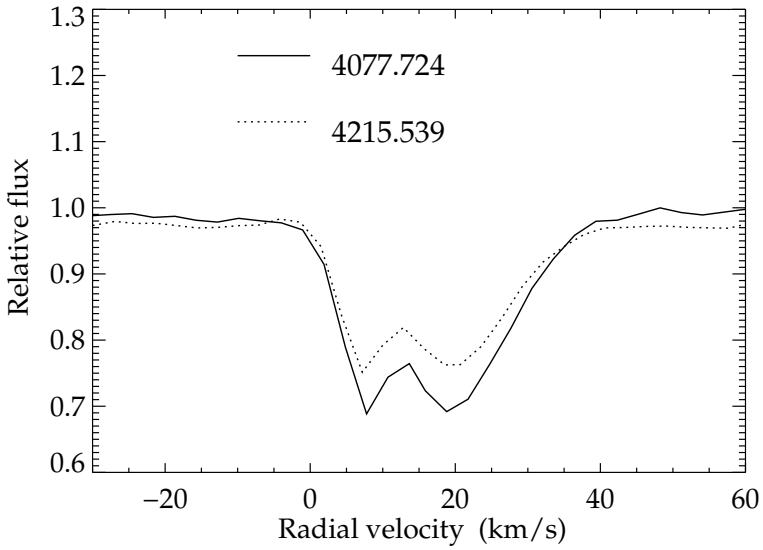

Fig. 5. Splitting of lines originating from low excitation levels in the spectrum of HD 52961. The lines of Sr II – $\lambda = 4077.7$ Å (solid line) and 4215.5 Å (dotted line) are plotted in the velocity scale.

of the blue components is $V_\mathrm{r} = 6.4 \pm 0.9$ km s^{-1}. With the D-lines included, $V_\mathrm{r} = 6.2 \pm 1.6$ km s^{-1}. The mean velocity of the red components is $V_\mathrm{r} = 19.5 \pm 2.0$ km s^{-1}. This velocity coincides with the mean velocity $V_\mathrm{r} = 18.9 \pm 0.4$ km s^{-1} derived from 302 non-split lines. The width (FWHM) of the blue components is about 6.4 ± 0.8 km s^{-1} which is much less than that of the red components, 22.4 ± 3.5 km s^{-1}. We also found 10 diffuse interstellar bands in the spectrum of HD 52961. Measured at the deepest points of their profiles, their mean velocity is about the same as that from the metallic lines. This is also the velocity one could expect if it is caused by the Galactic rotation at a distance of 2.1 kpc in the direction of HD 52961.

Most probably, the blue components are formed in the shell expanding with a velocity of about 12 km s^{-1}. The reddening caused by that matter is very small. From the D_2 blue component, using the calibration of Munari & Zwitter (1997), we found $E_{B-V} < 0.05$, Waelkens et al. (1991) for this star accepted $E_{B-V} = 0.04$.

The strong lines of C I are not split but show a marked asymmetry in the sense that their blue wings are stronger than the red ones. Using the Gaussian decomposition we measured the equivalent widths of extra blue absorptions of seven strong C I lines with equivalent widths greater than 10 pm. The Gaussian decomposition of strong C I lines was performed by the IRAF task "splot". It is illustrated for the C I $\lambda = 4932.05$ Å line in Figure 6.

These blue components have the equivalent widths of about 1 to 2 pm with the mean blue shift -23.4 ± 0.7 km s^{-1}, compared to the red components. From these numbers we derive the mass-loss rate almost in the same manner as Bakker et al. (1996) have done for HR 4049. From the luminosity $\log(L/L_\odot) = 3.7$ (see the next section), the assumed mass $M/M_\odot = 0.55$ (Waelkens et al. 1991), and the effective temperature $T_\mathrm{eff} = 6000$ K we found the stellar radius $R_* = 65 R_\odot$ and

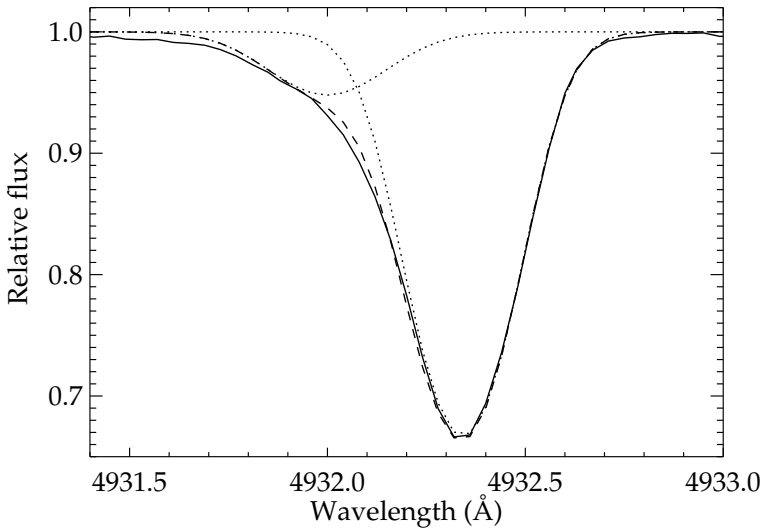

Fig. 6. Gaussian decomposition of the C I line $\lambda = 4932.05$ Å. Solid line – the observed profile, dotted line – the components at $\lambda = 4931.97$ Å with $W_\lambda = 1.7$ pm and FWHM = 37 pm, and at $\lambda = 4932.34$ Å with $W_\lambda = 12.2$ pm and FWHM = 35 pm. The sum of these components is indicated by the dashed line.

the terminal velocity $V_\infty = 85$ km s^{-1}. The terminal velocity is estimated from $V_\infty = 1.1 V_{\rm escape}$ (Lamers et al. 1995). With the CAK (Castor et al. 1975) wind velocity law, the velocity of 23.4 km s^{-1} is reached already at $r = 1.1 R_*$. Here we make another simplification and assume that the density in the atmosphere changes as $\rho \sim -2$. Consequently, we estimate $\dot{M} \approx 5 \cdot 10^{-6}\, M_\odot\, {\rm yr}^{-1}$. This mass-loss rate is at least an order of magnitude larger than is usually assumed for post-AGB stars. The blue components of the near-infrared Ca II split lines with the same procedure give about the same mass-loss rate if in addition we assume the same calcium abundance in the shell as in the photosphere. The estimates using the Ba II and Sr II lines give unrealistically large mass-loss rate indicating that the chemical composition of the gas, where these lines are formed, is not the same as in the photosphere.

2.4. Luminosity

The luminosity of HD 52961 calculated with the distance $d = 2.1 \pm 0.4$ kpc, derived by Gielen et al. (2011) from the SED fit, $E_{B-V} = 0.04$, and assuming the bolometric correction $BC = -0.1$, is $M_{\rm bol} = -4.5^{+0.7}_{-0.3}$ or $\log(L/L_\odot) = 3.7^{+0.2}_{-0.3}$. We also measured equivalent widths of the O I triplet lines at 7772–7775 Å. With the calibration by Arrellano Ferro et al. (2003) and $BC = -0.1$ the value of $M_{\rm bol}$ should be –5.8 mag.

Gielen et al. (2009) modeled the dusty disk of HD 52961 the presence of which has been proved by the interferometric observations with VLTI/MIDI instrument (Deroo et al. 2006). In order to fit the observed data to the model, they were forced to reduce the distance to HD 52961 to 1.6 ± 0.5 kpc and $\log L/L_\odot$ to 3.5. This luminosity is still in the range found above.

3. CONCLUSIONS

We have not found any appreciable changes in the chemical composition of HD 52961 during the 20 years which have passed from the first analyses of its atmosphere. We were able to estimate the rate of ongoing mass-loss $\dot{M} \approx 5 \cdot 10^{-6}\, M_{\odot}\, \mathrm{yr}^{-1}$. Even this strong mass-loss was insufficient to dissipate the metal-free atmosphere.

According to the scenario proposed by Waters et al. (1992), the selective accretion of metal-free gas occurs from a circum-system disk. Accretion from such a disc has the advantage since it can take place some time after the star has left AGB, as long as enough material is left in the disk. The stability of depleted from refractory elements photospheric composition seems to support this scenario. The formation of such a disk needs the presence of a companion. That HD 52961 is a binary system has been proved by Van Winckel et al. (1995, 1999). The presence of a dusty disk in the system was found by Deroo et al. (2006) who studied the system with mid-infrared long baseline interferometry with the VLTI/MIDI instrument. They found that the dust emission originates from a very small but resolved region which probably is trapped in the stable disk.

ACKNOWLEDGMENTS. This research was supported by a targeted financing project SF00600399S08 of the Estonian Ministry of Education and Research. This research is based on observations obtained on the Canada-France-Hawaii Telescope (CFHT) which is operated by the National Research Council of Canada, the Institut National des Sciences de l'Univers of the Centre National de la Recherche Scientique of France, and the University of Hawaii.

REFERENCES

Arellano Ferro A., Giridhar S., Rojo Arellano E. 2003, RMxAA, 39, 3
Asplund M., Grevesse N., Sauval A. J., Scott P. 2009, ARA&A, 47, 481
Bakker E. J., Van der Wolf F. L. A., Lamers H.J.G.L.M. et al. 1996, A&A, 306, 924
Castor J. I., Abbot D. C., Klein R. I. 1975, ApJ, 195, 157
Gielen C., Van Winckel H., Matsuura M. et al. 2009, A&A, 503, 843
Gielen C., Bowman J., Van Winckel H. et al. 2011, A&A, 533, 99
Deroo P., Van Winckel H., Min M. et al. 2006, A&A, 450, 181
Lamers H.J.G.L.M., Snow T. P., Lindholm D. 1995, ApJ, 455, 269
Lobel A. 2010, http://spectra.freeshell.org
Lodders K. 2003, ApJ, 591, 1220
Moore C. H., Minnaert M. G. J., Houtgast J. 1966, NBS Mono., 61
Munari U., Zwitter T. 1997, A&A, 318, 269
Ralchenko Yu., Kramida A. E., Reader J. & NIST ASD Team, 2011, NIST Atomic Spectra Database, http://physics.nist.gov/asd
Thévenin F. 1989, A&AS, 77, 137
Thévenin F. 1990, A&AS, 82, 179
Van Leeuwen F. 2007, A&A, 474,653
Van Winckel H., Waelkens C., Waters L.B.F.M. 1995, A&A, 293, L5
Van Winckel H., Waelkens C, Fernie I.D. & Waters L.B.F.M. 1999, A&A, 343, 202
Waelkens C., Van Winckel H., Bogaert E. 1990, ASPC, 11, 125
Waelkens C., Van Winckel H., Bogaert E., Trams N. R. 1991, A&A, 251, 495
Waters L.B.F.M., Trams N. R., Waelkens C. 1992, A&A, 262, L37

Table 4. Atomic data (wavelengths [Å], lower level excitation potentials ϵ_i [eV], oscillator strengths $\log gf$), equivalent widths [pm] and abundances calculated with the model parameters $T_{\rm eff} = 6000$ K, $\log g = 0.5$ and $\xi_{\rm t} = 6.8\,{\rm km\,s^{-1}}$ for HD 52961.

El.	λ	ϵ_i	$\log gf$	EW	$\log\varepsilon$	El.	λ	ϵ_i	$\log gf$	EW	$\log\varepsilon$
C I	4371.370	7.69	−1.96	9.5	8.24	C I	6683.970	8.85	−2.23	0.9	8.35
C I	4766.670	7.48	−2.62	5.5	8.38	C I	6688.790	8.85	−2.13	1.2	8.39
C I	4770.030	7.48	−2.44	7.3	8.37	C I	6711.320	8.54	−2.69	0.7	8.43
C I	4771.740	7.49	−1.87	14.0	8.30	C I	6828.120	8.54	−1.46	4.0	8.04
C I	4775.900	7.49	−2.30	8.5	8.33	C I	7056.890	8.64	−2.45	1.0	8.45
C I	4734.260	7.95	−2.37	3.3	8.26	C I	7074.860	8.64	−2.12	1.6	8.33
C I	4735.160	7.95	−3.11	0.7	8.29	C I	7076.480	8.64	−1.95	2.6	8.40
C I	4738.460	7.95	−2.64	2.5	8.40	C I	7085.479	8.64	−2.37	1.0	8.37
C I	4742.560	7.95	−2.99	0.9	8.28	C I	7087.830	8.65	−1.44	5.7	8.33
C I	4932.050	7.69	−1.66	13.2	8.20	C I	7093.240	8.65	−1.70	3.5	8.30
C I	5017.090	7.95	−2.46	2.8	8.27	C I	7100.120	8.64	−1.47	5.4	8.32
C I	5023.840	7.95	−2.21	4.9	8.32	C I	7108.930	8.64	−1.59	4.4	8.32
C I	5024.920	7.95	−2.73	1.8	8.33	C I	7111.470	8.64	−1.09	8.0	8.18
C I	5039.060	7.95	−1.79	8.6	8.24	C I	7113.180	8.65	−0.77	12.0	8.18
C I	5040.120	7.95	−2.30	3.8	8.27	C I	7115.170	8.64	−0.93	12.0	8.33
C I	5041.480	7.95	−2.00	6.5	8.27	C I	7116.990	8.65	−0.91	12.9	8.40
C I	5041.790	7.95	−2.06	6.2	8.30	C I	7119.770	8.64	−1.15	9.5	8.36
C I	5052.170	7.69	−1.30	17.6	8.16	C I	7132.110	8.65	−2.20	0.6	7.98
C I	5053.510	8.54	−2.06	1.7	8.14	C I	7473.310	8.77	−2.04	1.3	8.28
C I	5302.360	8.64	−2.50	0.9	8.39	C I	7476.180	8.77	−1.57	3.2	8.24
C I	5380.340	7.69	−1.62	13.4	8.19	C I	7483.450	8.77	−1.37	4.6	8.25
C I	5540.760	8.64	−2.38	0.7	8.17	C I	7832.680	8.85	−1.81	1.8	8.28
C I	5547.270	8.64	−2.25	1.3	8.32	C I	7837.100	8.85	−1.78	2.0	8.30
C I	5551.580	8.64	−1.90	2.1	8.19	C I	7848.200	8.85	−1.73	2.1	8.27
C I	5668.940	8.54	−1.47	5.2	8.15	C I	8015.000	8.85	−1.65	1.7	8.09
C I	5693.130	8.54	−1.85	1.4	7.87	C I	8045.340	8.85	−1.88	2.5	8.51
C I	5793.120	7.95	−2.06	5.2	8.23	C I	8058.620	8.85	−1.28	6.3	8.42
C I	5794.470	7.95	−2.79	1.7	8.39	C I	8062.360	8.85	−1.86	2.3	8.45
C I	5800.600	7.95	−2.34	3.5	8.29	C I	8078.480	8.85	−1.82	2.1	8.36
C I	5805.200	7.95	−2.68	1.9	8.33	C I	8083.790	8.85	−1.73	2.7	8.39
C I	6002.979	8.65	−2.17	0.9	8.09	C I	8753.070	9.00	−1.74	2.5	8.31
C I	6007.180	8.64	−2.06	1.7	8.27	C I	8873.360	9.00	−1.14	5.9	8.17
C I	6010.650	8.64	−1.94	2.3	8.29						
C I	6012.230	8.64	−2.01	1.4	8.13	N I	7442.290	10.32	−0.40	3.0	7.91
C I	6014.840	8.64	−1.58	3.9	8.21	N I	7468.310	10.34	−0.18	4.2	7.90
C I	6016.450	8.64	−1.83	1.7	8.04	N I	8594.000	10.68	−0.34	2.7	7.84
C I	6078.390	8.85	−2.27	0.6	8.19	N I	8629.240	10.69	0.08	6.2	7.93
C I	6108.520	8.85	−2.51	0.6	8.43	N I	8655.890	10.69	−0.62	1.9	7.93
C I	6115.840	8.85	−2.51	0.5	8.35	N I	8683.400	10.33	0.11	8.8	7.85
C I	6120.810	8.85	−2.41	0.6	8.33	N I	8686.150	10.33	−0.28	6.0	7.96
C I	6397.970	8.77	−1.78	1.2	7.96	N I	8703.250	10.33	−0.31	5.0	7.88
C I	6413.550	8.77	−2.00	1.0	8.09	N I	8711.700	10.33	−0.23	6.2	7.94
C I	6587.610	8.54	−1.00	11.1	8.23	N I	8718.840	10.34	−0.35	5.3	7.96
C I	6591.460	8.85	−2.41	0.4	8.16	N I	8728.900	10.33	−1.07	1.3	7.91
C I	6611.350	8.85	−1.84	1.6	8.23						
C I	6654.610	9.00	−2.02	1.1	8.37	O I	4368.240	9.52	−1.96	2.0	8.60
C I	6655.520	8.54	−2.00	2.9	8.40	O I	4773.750	10.74	−1.67	0.4	8.58
C I	6671.850	8.85	−1.65	1.9	8.12	O I	5329.680	10.74	−1.23	0.8	8.53
C I	6674.200	8.85	−2.23	1.0	8.40	O I	6155.980	10.74	−1.01	2.2	8.89
C I	6679.640	8.85	−2.35	0.8	8.42	O I	6156.780	10.74	−0.69	2.6	8.66

Table 3. Continued

El.	λ	ϵ_i	$\log gf$	EW	$\log \varepsilon$	El.	λ	ϵ_i	$\log gf$	EW	$\log \varepsilon$
O I	6158.180	10.74	−0.41	3.2	8.50	Ca II	3933.660	0.00	0.14	60.8	2.15
O I	6454.439	10.74	−1.07	0.7	8.45	Ca II	3968.450	0.00	−0.18	0.0	12.09
O I	6455.980	10.74	−0.92	1.0	8.46	Ca II	8542.090	1.70	−0.36	54.0	2.91
O I	9262.770	10.74	0.64	18.3	8.57	Ca II	8662.140	1.69	−0.62	43.3	2.42
O I	9266.030	10.74	0.81	20.0	8.49	Ca II	8498.020	1.69	−1.32	0.0	12.23
Na I	4978.540	2.10	−1.22	0.5	5.00	Sc II	4246.820	0.32	0.24	0.6	−1.76
Na I	4982.810	2.10	−0.96	0.9	5.01						
Na I	5682.630	2.10	−0.71	1.8	5.06	Ti II	3900.540	1.13	−0.20	1.5	0.28
Na I	5688.210	2.10	−0.45	3.2	5.07	Ti II	4028.350	1.89	−0.99	1.3	1.71
Na I	8183.260	2.10	0.24	10.5	5.02	Ti II	4468.490	1.13	−0.62	0.2	−0.26
Na I	8194.820	2.10	0.49	15.6	5.08	Ti II	4571.970	1.57	−0.32	0.3	0.03
						Ti II	5185.910	1.89	−1.37	0.2	1.16
Mg I	5172.700	2.71	−0.39	3.2	3.58	Ti II	5381.020	1.57	−1.97	0.8	2.07
Mg I	5183.620	2.72	−0.18	4.3	3.52						
Mg I	5167.320	2.71	−0.87	1.5	3.71	Cr II	4558.650	4.07	−0.45	0.4	1.85
						Cr II	4588.200	4.07	−0.63	0.3	1.84
Si I	3905.520	1.91	−1.04	2.8	3.51						
						Mn I	4030.760	0.00	−0.97	2.1	2.22
S I	3962.000	6.52	−2.11	0.9	6.42	Mn I	4033.070	0.00	−1.04	2.7	2.50
S I	4152.600	6.86	−1.94	1.2	6.66						
S I	4157.700	6.86	−1.69	2.1	6.67	Fe I	4045.820	1.49	0.28	2.1	2.80
S I	4694.110	6.52	−1.71	3.2	6.56	Fe I	4202.030	1.49	−0.71	0.3	2.90
S I	4695.440	6.52	−1.87	2.4	6.59	Fe I	4271.760	1.49	−0.16	1.5	3.06
S I	4696.250	6.52	−2.10	1.4	6.57	Fe I	4383.540	1.49	0.20	2.3	2.88
S I	6041.930	7.87	−1.10	1.7	6.86	Fe I	4404.750	1.56	−0.14	0.9	2.86
S I	6046.040	7.87	−0.82	2.4	6.74	Fe I	4415.120	1.61	−0.62	0.6	3.20
S I	6052.660	7.87	−0.64	3.2	6.70	Fe I	4920.500	2.83	0.07	0.1	2.84
S I	6403.570	7.87	−1.67	0.3	6.65						
S I	6415.479	7.87	−1.30	0.4	6.41	Fe II	4522.630	2.84	−2.03	0.6	3.15
S I	7443.350	8.42	−0.55	1.1	6.62	Fe II	4583.840	2.81	−1.86	0.9	3.13
S I	7447.700	8.42	−1.15	0.4	6.76	Fe II	4923.920	2.89	−1.32	2.1	3.04
S I	7696.720	7.87	−0.91	1.8	6.70						
S I	7930.280	8.42	−0.68	0.9	6.65	Ni I	3984.150	3.68	−0.19	0.4	4.18
S I	8626.630	8.41	−0.89	0.7	6.59	Ni I	7122.200	3.54	−0.05	0.6	3.97
S I	8633.200	8.41	−0.42	2.2	6.64						
S I	8655.170	8.41	−0.92	1.1	6.82	Zn I	4810.530	4.08	−0.14	4.1	3.13
S I	8670.650	7.87	−0.56	3.2	6.47	Zn I	4722.150	4.03	−0.34	3.3	3.18
S I	8671.310	7.87	−0.66	2.6	6.47						
S I	8694.710	7.87	0.05	10.7	6.55	Sr II	4077.720	0.00	0.15	8.4	−1.63
S I	8884.200	8.42	−0.18	3.0	6.55	Sr II	4215.540	0.00	−0.17	6.0	−1.52
						Ba II	4554.030	0.00	0.14	1.1	−2.19
						Ba II	4934.090	0.00	−0.16	0.8	−2.06